Supporting Information

Hydroxyl-Oxygen Vacancy Synergy over In_2O_3-ZrO_2 Catalysts: Mechanistic Insights into CO_2 Hydrogenation to Methanol

Xia Li[a,†], Zixia Feng[b,†], Hanjun Lu[a], Xinlin Hong[a,*],Guangchao Li[b,c,d,*], Shik Chi Edman Tsang[b,c,d]

---

[a] *College of Chemistry and Molecular Sciences; Wuhan University; Wuhan 430072, China, E-mail: hongxl@whu.edu.cn.*

[b] *Department of Applied Biology and Chemical Technology, The Hong Kong Polytechnic University, Hong Kong 999077, China,*

[c] *The Hong Kong Polytechnic University Shenzhen Research Institute, The Hong Kong Polytechnic University, Shenzhen 518057, China*

[d] *PolyU-Daya Bay Technology and Innovation Research Institute, The Hong Kong Polytechnic University, Huizhou 516000, China*

[e] *Research Institute of Advanced Manufacturing (RIAM), Research Centre for Resources Engineering towards Carbon Neutrality (RCRE), The Hong Kong Polytechnic University, Hong Kong 999077, China*

E-mail: guangchao.li@polyu.edu.hk

† X Li and Z Feng contributed to this paper equally.

Methods

Synthesis of ZrO_2 support. Amorphous ZrO_2 was prepared via using a gel-assisted solvothermal method, similar to that we reported previously.[1] Briefly, 6.0g $Zr(NO_3)_4{\cdot}5H_2O$ were dissolved in 50 mL ethanol. Subsequently, propylene oxide was gradually added to this solution under continuous stirring, which was kept in stirring for 2 min. The resultant transparent sol was then transferred into a Teflon-lined stainless-steel autoclave and subjected to a solvothermal treatment at 150 °C for 20 h. Upon cooling to room temperature, the formed gel was dried at 60 °C for 24 hours and further calcined in air at 200 °C for 3 hours. Finally, to obtain ZrO_2 carriers with different monoclinic contents, amorphous zirconia was calcined at 300 °C, 400 °C, 600 °C, and 800 °C with a heating rate of 2 °C min^{-1}, respectively. The obtained support was marked as Zr300, Zr400, Zr600 and Zr800.

Synthesis of In_2O_3-ZrO_2 catalysts. In_2O_3-ZrO_2 catalysts were synthesized using the impregnation method. All catalysts were represented as xIn_aZr_b, where x represents the mass fraction of In (x%). Typically, $In(NO_3)_3{\cdot}4H_2O$ was dissolved in water, and a certain volume of $In(NO_3)_3{\cdot}4H_2O$ solution was added to 0.2 g of the ZrO_2 support according to the mass fraction of In. The mixture was kept for 2 h at room temperature under constant stirring, completely dried by rotary evaporation, and then calcined at a °C in the air. All In_2O_3-ZrO_2 catalysts were calcined at 300 °C except Zr300 calcined at 400 °C after impregnation.

Catalytic testing

The evaluation of the catalyst was conducted in a fixed-bed reactor with an inside diameter of 6 mm. Before the test, 0.1 g precursor catalysts were mixed with 0.4 g quartz sand (40-60 mesh) and reduced in a 10 vol % H_2/Ar stream (10 mL min^{-1}) at 350 °C for 1 h under atmospheric pressure. Next, a feed gas of ($CO_2/H_2=1/3$ by volume, 4 vol% N_2 as an internal standard, and GHSV of 12000 mL $gcat^{-1}$ h^{-1}) was inducted into the reactor and the pressure was increased 5.0 MPa. Subsequently, the catalytic activity was carried out at different target temperatures (250, 270, 290 and 310 °C). The effluent products were monitored online using a gas chromatograph, equipped with a thermal conductivity detector (TCD, TDX-01 column) and a flame ionization detector (FID, CB-Plot Q capillary column). The long-term stability was evaluated by a test of stability (TOS) test at 310 °C, 5 MPa, 12000 mL $gcat^{-1}$ h^{-1} for 100 h.

The CO_2 conversion, CO selectivity, Methanol selectivity were calculated according to the following equations 1-3:

$$f = \frac{C}{A} \qquad \text{(Eq 1)}$$

$$CO_2\ Conversion = \frac{A_{CO_2,\,\mathrm{in}} A_{CO_2,out}}{A_{CO_2,\mathrm{in}}} \times 100\% \qquad \text{(Eq 2)}$$

$$\text{Selectivity} = \frac{N_i \times A_{i,out} \times f_i}{(A_{CO_2,\mathrm{in}} A_{CO_2,out}) \times f_{CO_2}} \times 100\%$$

(Eq 3)

where f is the relative correction factor defined as C/A and C represents the concentration related to reactants or products. $A_{CO2,in}$ and $A_{CO2,out}$ stand for chromatographic peak areas of carbon dioxide at the inlet and outlet, respectively. N_i and $A_{i,out}$ denote the carbon moles and chromatographic peak areas of the carbon products (i) at the outlet.

Characterization.

H_2-TPR measurements. Temperature-programmed reduction of H_2 (H_2-TPR) were measured by using a Micromeritics Autochem 2920. Typically, 50 mg of catalyst was placed into a U-type quartz tube and pre-treated in a high purity Ar gas (30 mL min^{-1}) at 150 °C for 1 h. After cooled down to room temperature, the gas was switched into 5 vol% H_2/Ar (30 mL min^{-1}) and the tube was purged for 10 min. After that, the sample temperature was ramped up to 900 °C with a heating rate of 10 °C min^{-1}, and a TCD (thermal conductivity detector) recording was simultaneously started.

CO_2-TPD measurements. Temperature-programmed desorption with CO_2 (CO_2-TPD) were done on Micromeritics AutoChem 2920 apparatus with an on-line Hiden QIC-20 mass spectrometer. Briefly, 50mg of catalyst was pretreated with 5 vol% H_2/Ar at 350 °C for 1 h and cooled to 50 °C. Afterwards, the pretreated catalyst was exposed to pure CO_2 at 50 °C for 30 min and then purged with Ar flow at the same temperature to eliminate all physiosorbed CO_2. After 1 h purging, the temperature was raised from 50 to 900 °C (10 °C min^{-1} ramp rate) as CO_2 desorption (m/z signal = 44) was monitored by mass spectrometer.

NH_3-TPD measurements. Temperature-programmed desorption with NH_3 (NH_3-TPD) were done on Micromeritics AutoChem 2920 apparatus with an on-line Hiden QIC-20 mass spectrometer. Briefly, 50mg of catalyst was exposed to pure NH_3 at 50 °C for 60 min and then purged with Ar flow at the same temperature to eliminate all physiosorbed NH_3. After 1 h purging, the temperature was raised from 50 to 900 °C (10 °C min^{-1} ramp rate) as CO_2 desorption (m/z signal = 44) was monitored by mass spectrometer.

Material characterization. XRD patterns were obtained on a Rigaku Miniflex600 (Japan) X-ray diffractometer with a Cu Kα (λ = 0.15406 nm) radiation source. Brunauer-Emmett-Teller (BET) surface area and pore structure were analyzed on a Micromeritics ASAP-2020 automatic N_2 adsorption system (America). The loading of In and Zr was measured by inductively coupled plasma-atomic emission spectrometry (ICP-OES) on an IRIS Intrepid II XSP instrument. X-ray photoelectron spectra (XPS) were carried out on a Thermo Scientific ESCALAB 250Xi X-ray photoelectron spectrometer with a monochromatic Al Kα source (hν = 1486.6 eV) with an operating power of 150 W (15 kV, 10 mA). High-angle annular dark-field scanning transmission electron microscopy (HAADF-STEM) and energy-dispersive X-ray spectroscopy (EDS) analyses were conducted utilizing a spherical aberration-corrected transmission electron microscope (FEI Titan Themis) functioning at an accelerating potential of 300 kV.

The solid-state NMR (SSNMR) measurements

^1H MAS SSNMR measurements were conducted using solid-state nuclear magnetic resonance (SSNMR) experiments on a JEOL ECZ500R spectrometer. The resonance frequency for the ^1H nucleus was 495.13 MHz. Spectral deconvolution was performed using Delta software. The ^1H magic-angle spinning (MAS) SSNMR spectra were acquired using a 3.2 mm probe with a spinning rate of 12 kHz, a pulse width of 2.95 μs (approximately a $\pi/2$ pulse), a recycle delay of 5 s, and 32 scans.

TMP-assisted ^{31}P MAS SSNMR Analysis. ^{31}P MAS SSNMR measurements were performed using solid-state nuclear magnetic resonance (SSNMR) experiments on a JEOL ECZ500R spectrometer. The resonance frequency for the ^{31}P nucleus was 200.43 MHz. Spectral deconvolution was performed using Delta software. The ^{31}P MAS SSNMR experiments were conducted on a 4 mm probe with a spinning frequency of 10 kHz. A total of 4400 scans were accumulated to collect the ^{31}P MAS SSNMR spectra, with a pulse width of 2.77 μs (corresponding to a $\pi/2$ flip angle), a recycle delay of 30 s, a contact time of 2 ms, and a recycle delay of 2 s.

High-resolution 1D ^{13}C SSNMR and 2D ^{13}C-^1H HETCOR MAS SSNMR spectra were acquired using a JEOL ECZ500R spectrometer. The resonance frequencies for the ^{13}C and ^1H nuclei were 124.50 MHz and 495.13 MHz, respectively. The MAS spinning rate was set to 10 kHz to ensure high-resolution spectra. For 1D ^{13}C SSNMR: The 90° pulse width was 2.8 μs. The spectral width was set to 150 ppm to cover the entire chemical shift range of the ^{13}C nucleus. A recycle delay of 5 s was employed to ensure complete relaxation of the ^{13}C spins between successive scans. A total of 1024 scans were accumulated to achieve a satisfactory signal-to-noise ratio (SNR). For 2D ^{13}C-^1H HETCOR MAS SSNMR: A cross-polarization (CP) sequence was used with a contact time of 2 ms. The spectral widths were set to 1 ppt for ^{13}C and 30 ppm for ^1H. A recycle delay of 2 s was used, and 64 scans were accumulated in the indirect dimension.

In situ DRIFTS Measurements.

In situ DRIFTS spectra of the CO_2+H_2 reaction. *In situ* DRIFTS spectra were measured on a Bruker VERTEX 70 (Bruker, Germany) equipped with an MCT detector, operating at a resolution of 4 cm^{-1} with 64 scans. Prior to the measurements, 10 mg catalyst was loaded into the *in situ* IR cell and subjected to a pre-reduction treatment. The 10In300Zr400 catalyst was reduced in a 10 vol% H_2/Ar atmosphere (30 mL min^{-1}) at 350 °C for 1 h, with a heating rate of 5 K min^{-1}. Subsequently, the reactor was purged with high-purity Ar (30 mL min^{-1}) for 1 h. Background spectra were collected at the desired temperatures (100, 200, 250, and 300 °C) after cooling to each target temperature. Then the reaction was initiated by introducing a CO_2/H_2 mixture (1:3 by volume) into the reactor at a flow rate of 30 mL min^{-1} under a pressure of 1 MPa, while simultaneously recording the time-resolved DRIFTS spectra.

In situ DRIFTS spectra of the H_2 reduction. 10 mg of catalyst was loaded into an *in situ* IR cell. High-purity argon (Ar) was introduced at a constant flow rate of 30 mL/min, and the temperature was increased to 350 °C at a heating rate of 5 K/min. After maintaining the system at 350 °C for 1 h under Ar flow, the infrared background spectrum was recorded. Subsequently, the gas stream was switched to a 10% H_2/Ar mixture, maintaining the same flow rate (30 mL/min). Simultaneously, time-resolved in situ infrared spectroscopy measurements were initiated. The infrared spectra were collected in the range of 1000-4000 cm^{-1} with a spectral resolution of 4 cm^{-1}, accumulating 64 scans per spectrum.

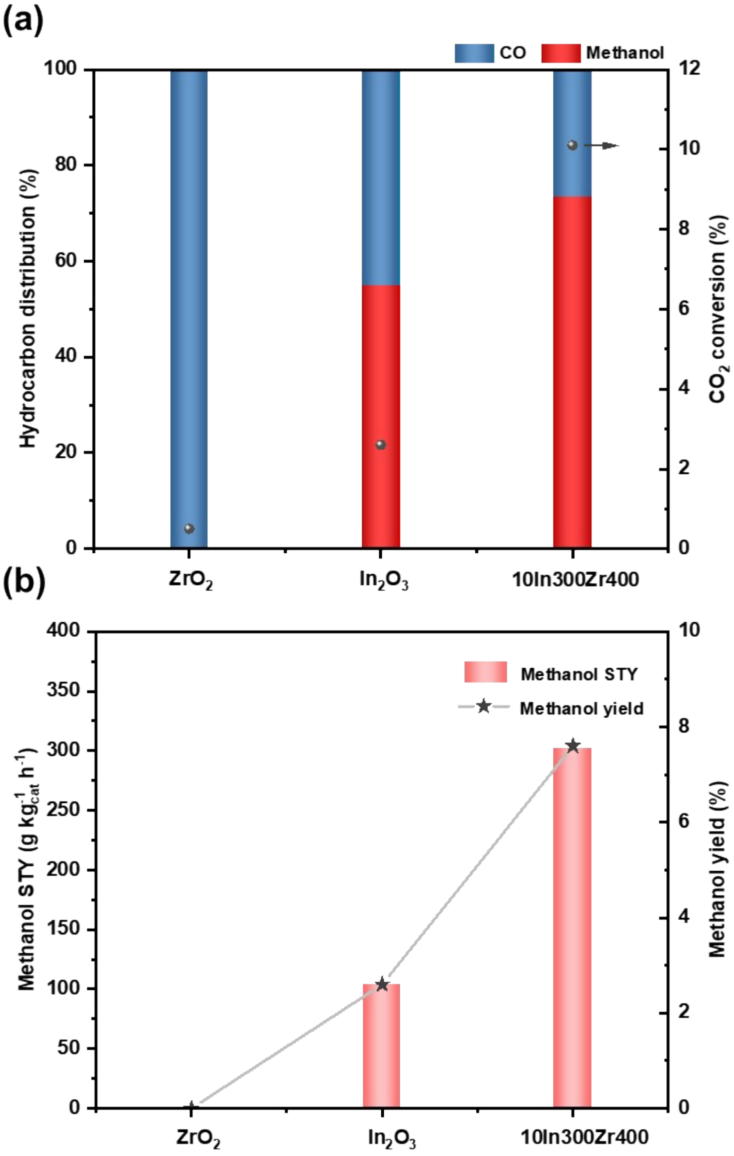

Figure S1. Catalytic performance of ZrO_2, In_2O_3, 10In300Zr400 (a) CO_2 conversion and product distribution and (b) space-time yield (STY) of methanol. Reaction conditions: 0.1g catalyst, GHSV=12000 mL g_{cat}^{-1} h^{-1}, 5MPa, 310 °C, $H_2/CO_2=3$.

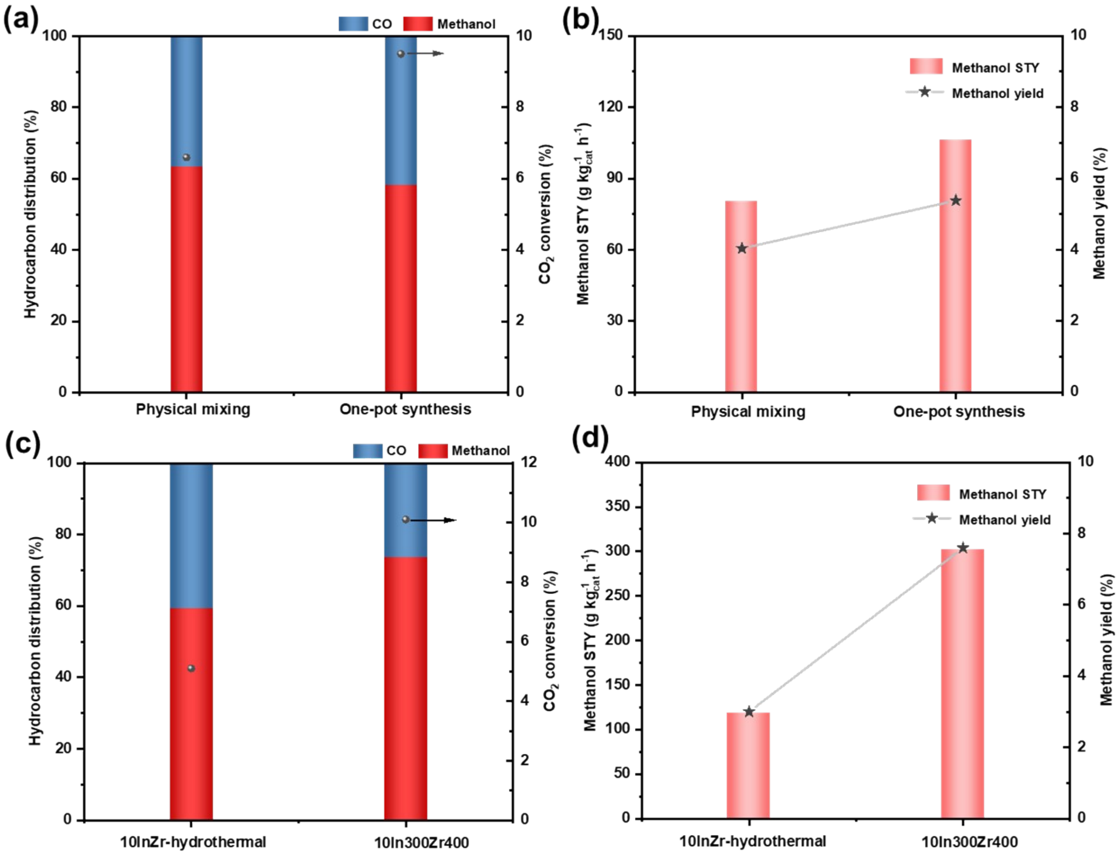

Figure S2. Catalytic performance of catalysts via physical mixing, one-pot synthesis, 10InZr-hydrothermal and 10In300Zr400. (a, c) CO_2 conversion and product distribution and (b, d) space-time yield (STY) of methanol. Reaction conditions:(a, b) 0.1g catalyst, GHSV=6000 mL g_{cat}^{-1} h^{-1}, 3MPa, 300 °C, H_2/CO_2=3; (c, d) 0.1g catalyst, GHSV=12000 mL g_{cat}^{-1} h^{-1}, 5MPa, 310 °C, H_2/CO_2=3.

As shown in Figure S2, the physical mixed catalysts of 10In/t-ZrO_2 and 10In/m-ZrO_2 were prepared by blending the corresponding proportions of t-ZrO_2 and m-ZrO_2, which were determined based on the content of m-ZrO_2 and t-ZrO_2 in the 10In300Zr400 synthesized via a one-pot method.

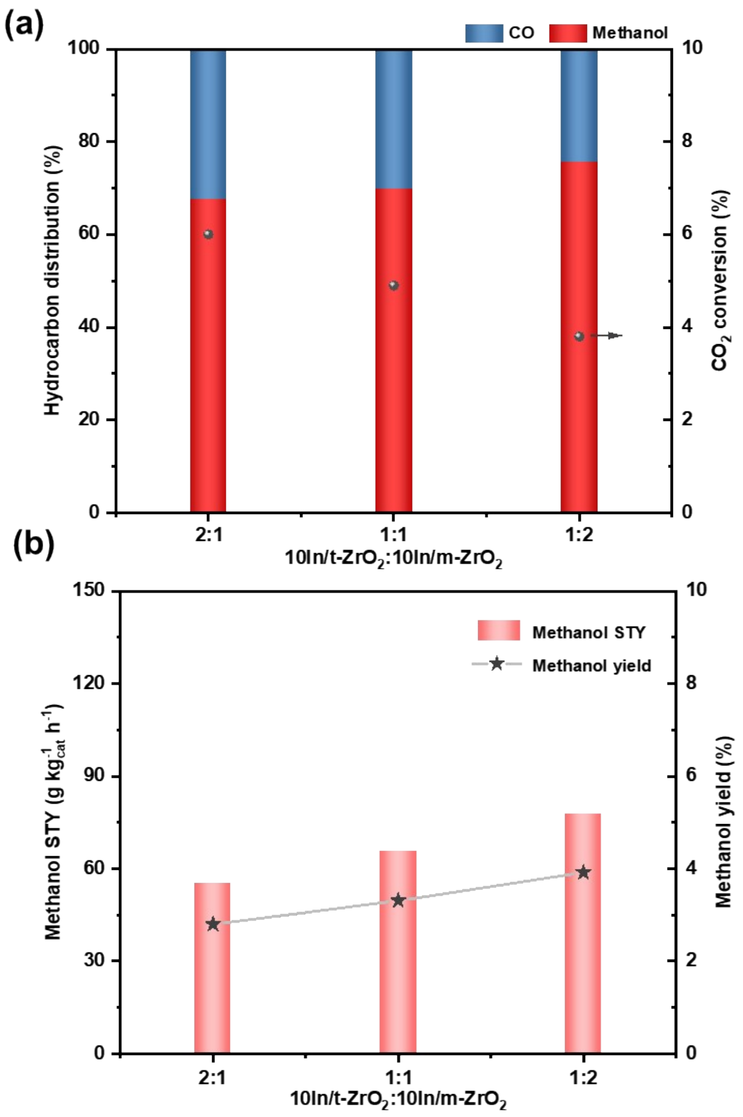

Figure S3. Catalytic performance of the catalysts prepared by physical mixing with varying mass ratios of 10In/t-ZrO_2 and 10In/m-ZrO_2. (a) CO_2 conversion and product distribution and (b) space-time yield (STY) of methanol. Reaction conditions: 0.1g catalyst, GHSV=6000 mL g_{cat}^{-1} h^{-1}, 3MPa, 300 °C, H_2/CO_2=3.

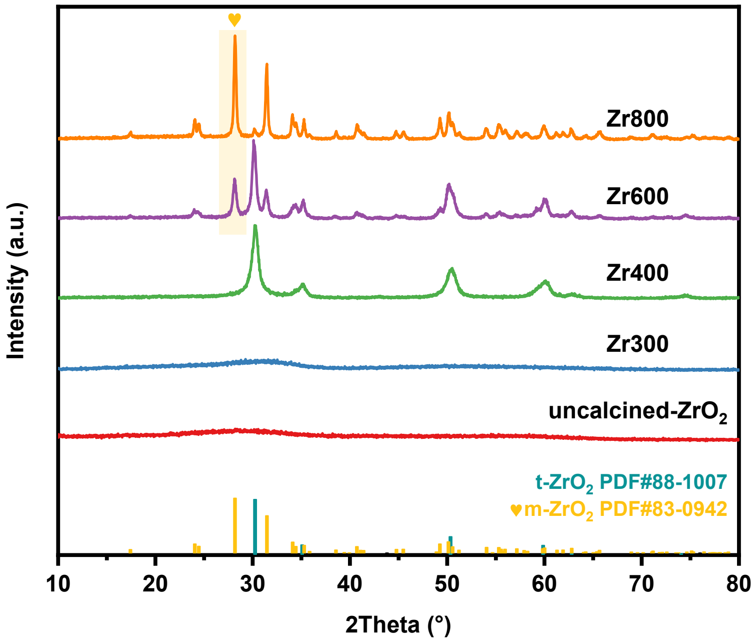

Figure S4. XRD patterns of ZrO_2 supports calcined at different temperatures.

Figure S4 shows the powder diffraction profiles of a-ZrO_2 after calcination in the range of 300-800 °C and labeled as Zrx, where x represents the calcination temperature. Zr300 remains amorphous with a diffuse scattering halo ca. 30°. When the temperature reaches 400 °C, the bare carrier is completely transformed into a metastable tetragonal phase with a characteristic peak (101) at ~30.2° (PDF#88-1007). The strong diffraction peak (-111) of m-ZrO_2 at ~28.2° is more visible in the carrier with a further increase in temperature.

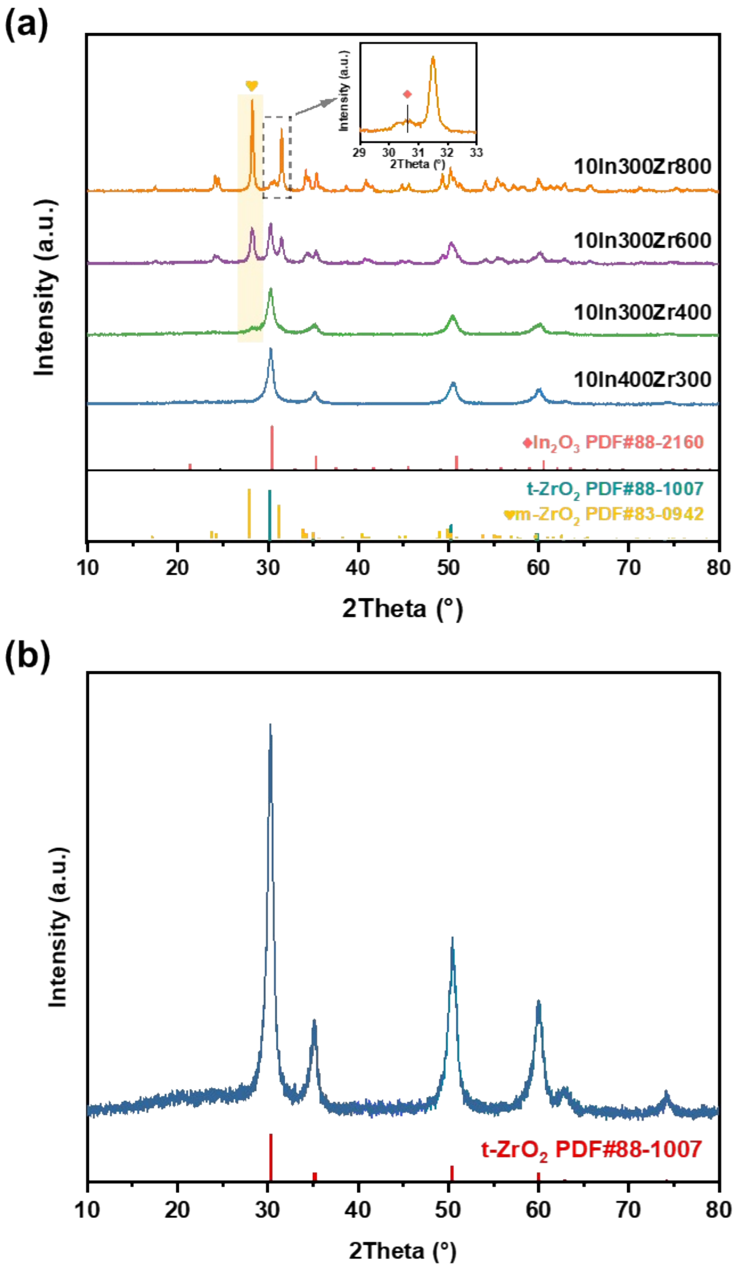

Figure S5. XRD patterns of In_2O_3-ZrO_2 catalysts (a) and 10InZr-hydrothermal (b).

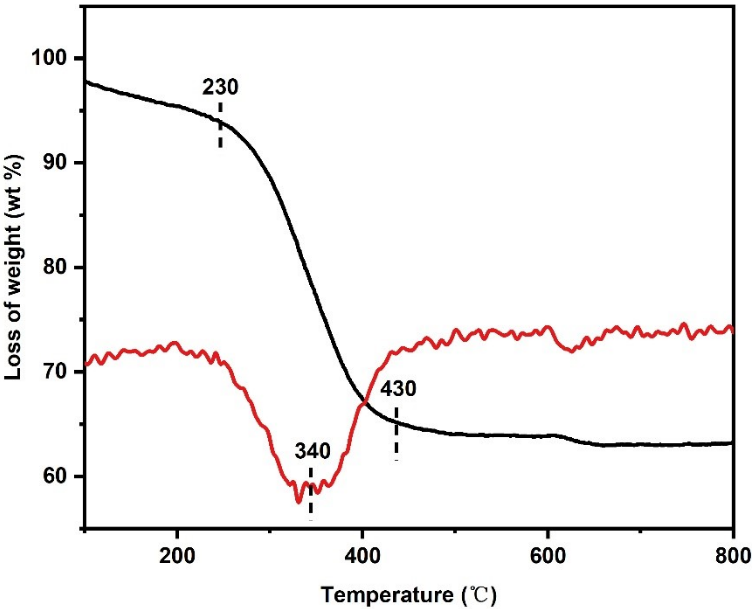

Figure S6. TGA-DTG profiles of amorphous ZrO_2.

TGA-DTG analysis illuminates the thermal decomposition behavior of a-ZrO_2. The mass loss on the TG curve occurs below about 110 °C and 230-430 °C corresponds to the removal of physically adsorbed water and crystalline water. m-ZrO_2 is the most stable morphology at room temperature. Conversely, t-ZrO_2 is metastable at low temperatures, but when the temperature increases, it undergoes a crystalline phase transition to a stable monoclinic crystal structure. And this crystalline phase transition is mainly attributed to the condensation of surface hydroxyls.

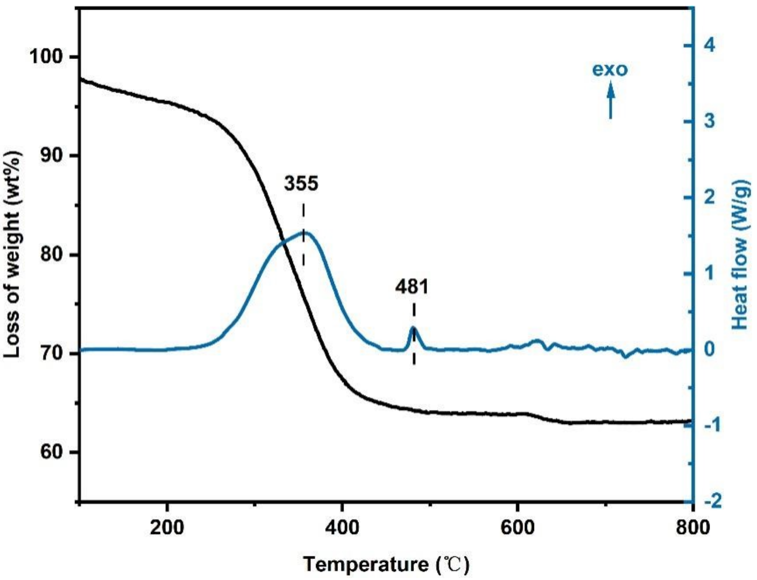

Figure S7. TGA-DSC profiles of amorphous ZrO_2.

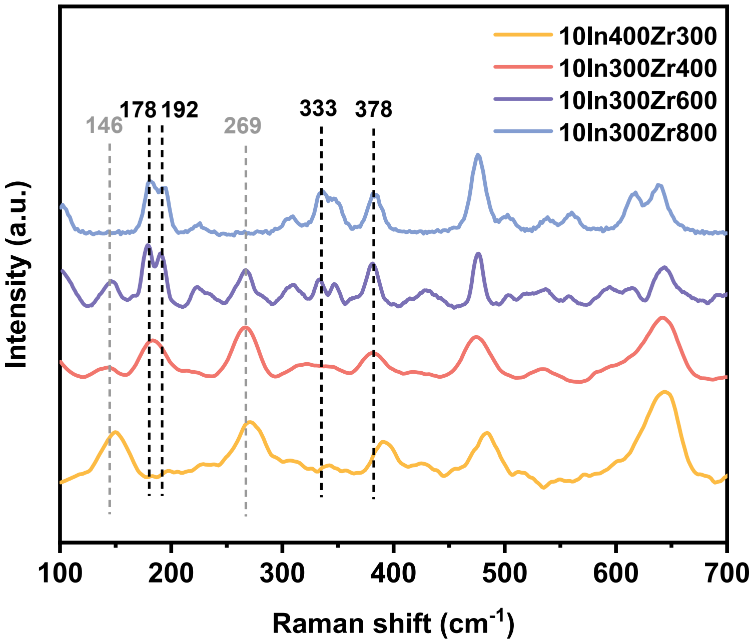

Figure S8. Raman spectra of catalysts with a 532 nm laser.

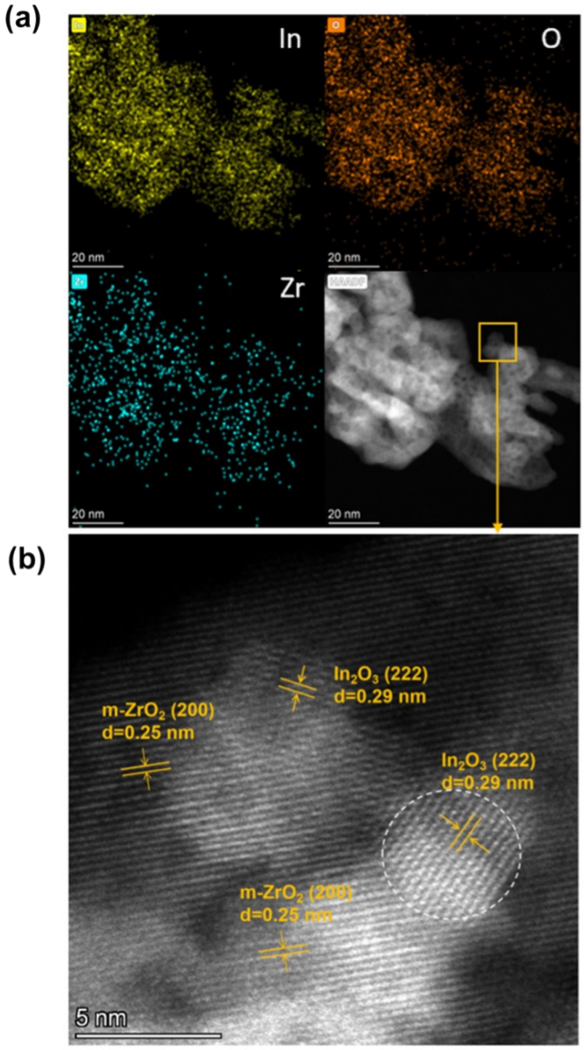

Figure S9. EDX elemental mapping of fresh-10In3000Zr600 (a) and HAADF-STEM images of fresh-10In3000Zr600

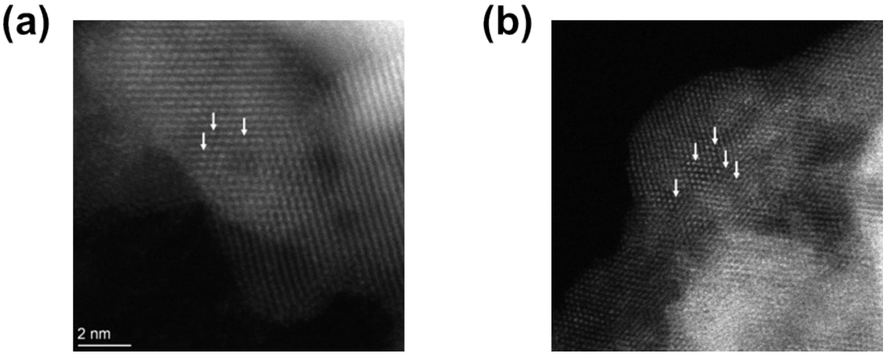

Figure S10. Aberration-corrected HAADF-STEM images of fresh-10In3000Zr400 (a) and spent 10In300Zr400 (b).

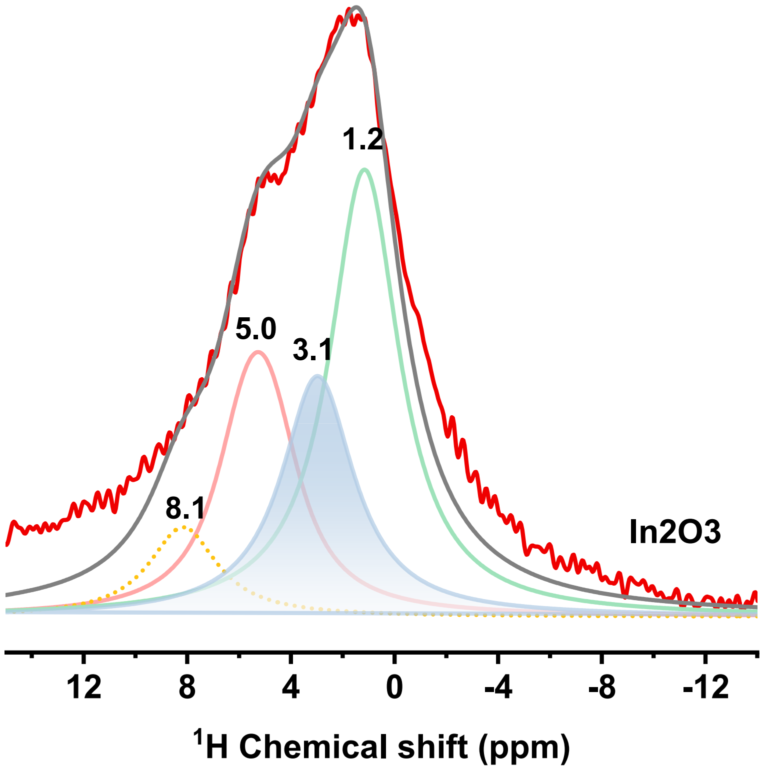

Figure S11. ^{1}H MAS SSNMR spectra of In_2O_3.

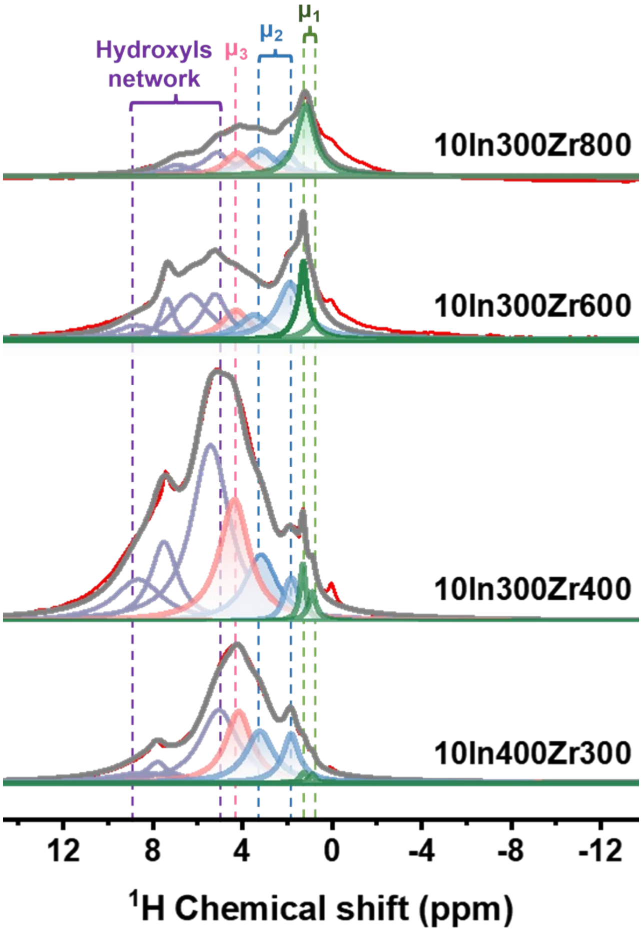

Figure S12. ^{1}H MAS SSNMR spectra of In_2O_3-ZrO_2 catalysts.

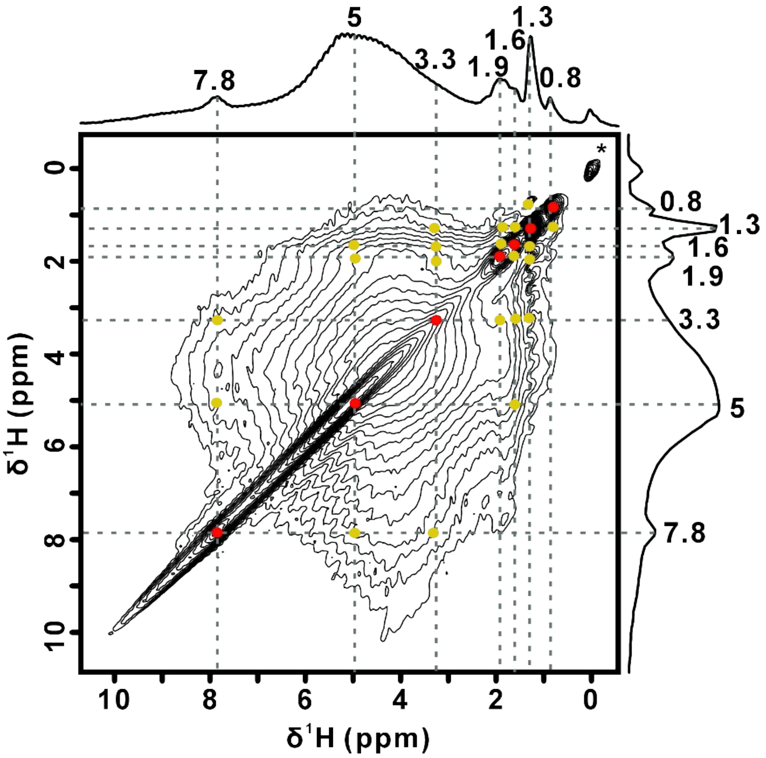

Figure S13. 2D ^{1}H-^{1}H homonuclear correlation SSNMR spectra of 10In400Zr300.

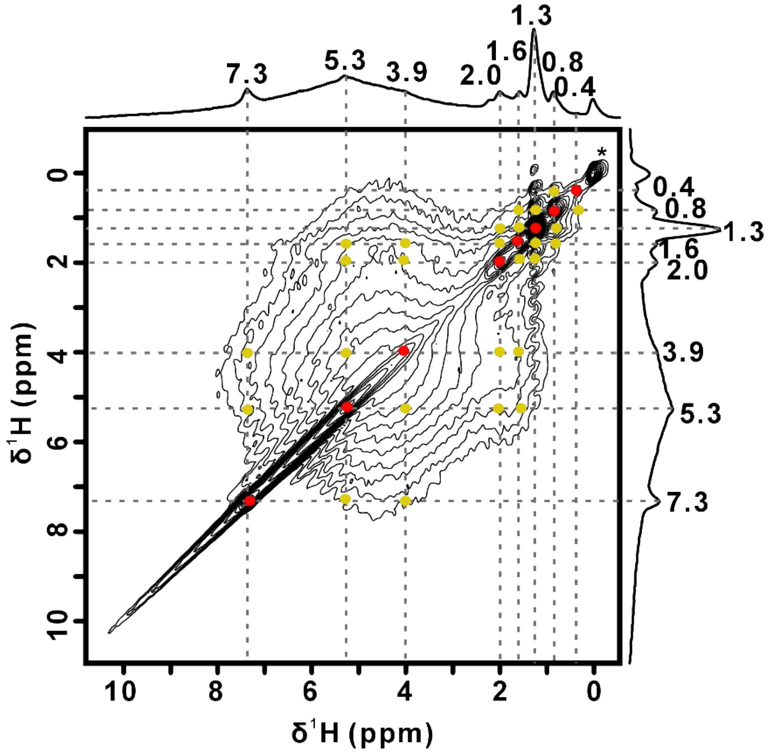

Figure S14. 2D ^{1}H-^{1}H homonuclear correlation SSNMR spectra of 10In300Zr600.

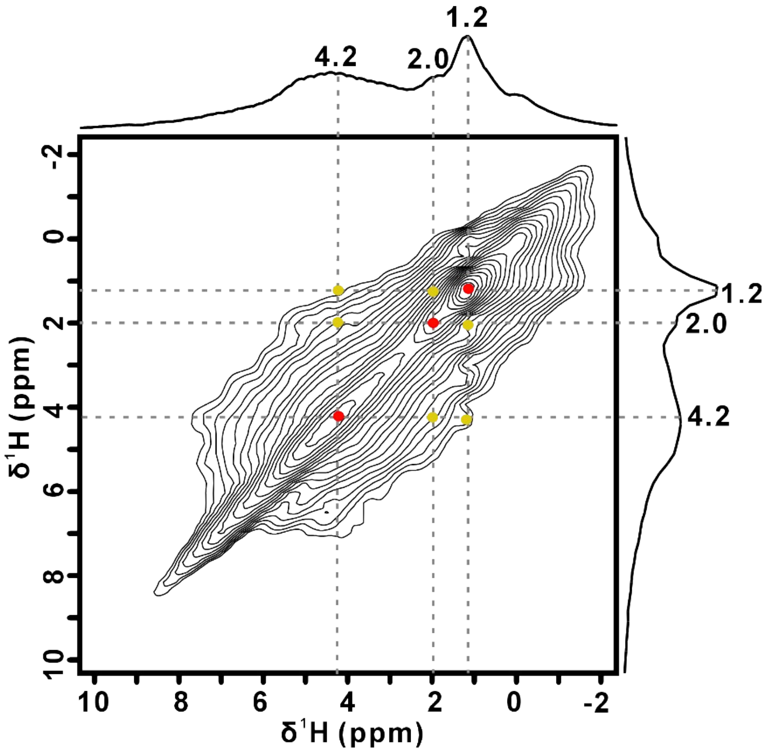

Figure S15. 2D ^{1}H-^{1}H homonuclear correlation SSNMR spectra of 10In300Zr800.

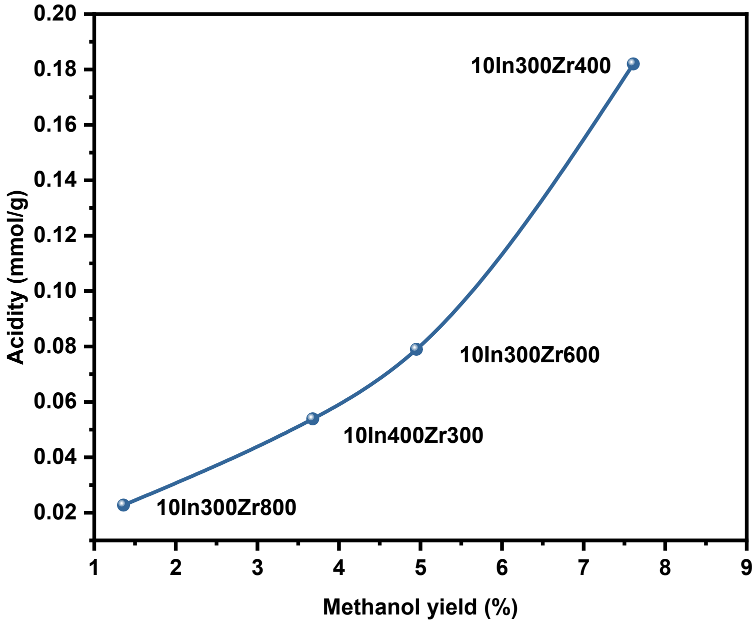

Figure S16. The proportion of acidity and methanol yield for CO_2 hydrogenation over In_2O_3-ZrO_2 catalysts. Reaction condition: 0.1g catalyst, GHSV=12000 mL g_{cat}^{-1} h^{-1}, 5MPa, 310 °C, H_2/CO_2=3.

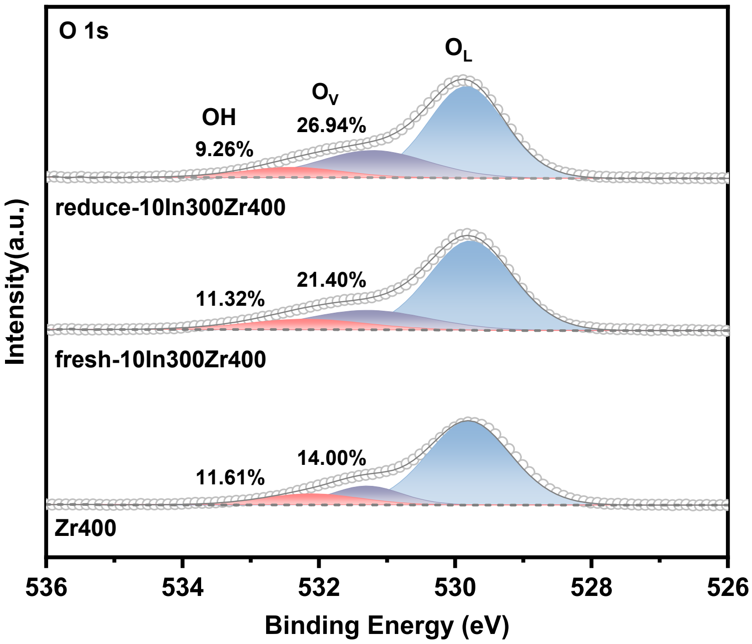

Figure S17. O1s XPS spectra of Zr400, fresh and reduce 10In300Zr400 catalysts.

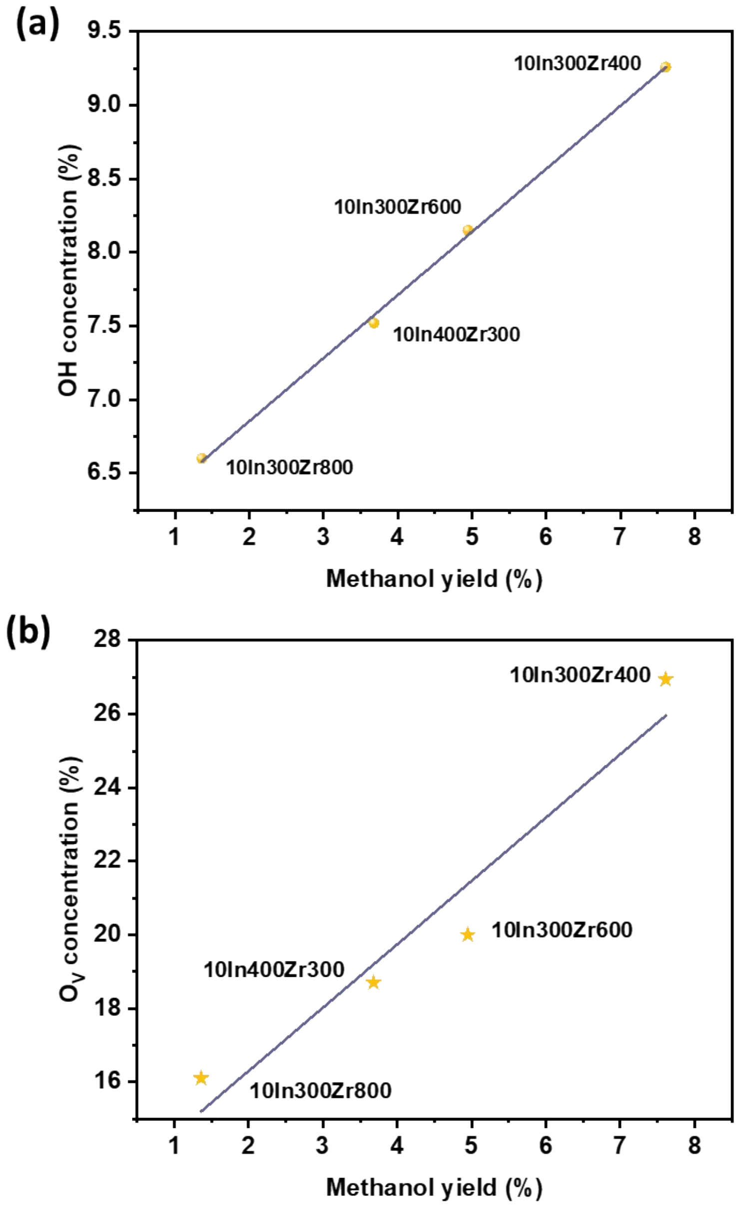

Figure S18. the proportion of OH/O_V concentration and methanol yield for CO_2 hydrogenation over In_2O_3-ZrO_2 catalysts.

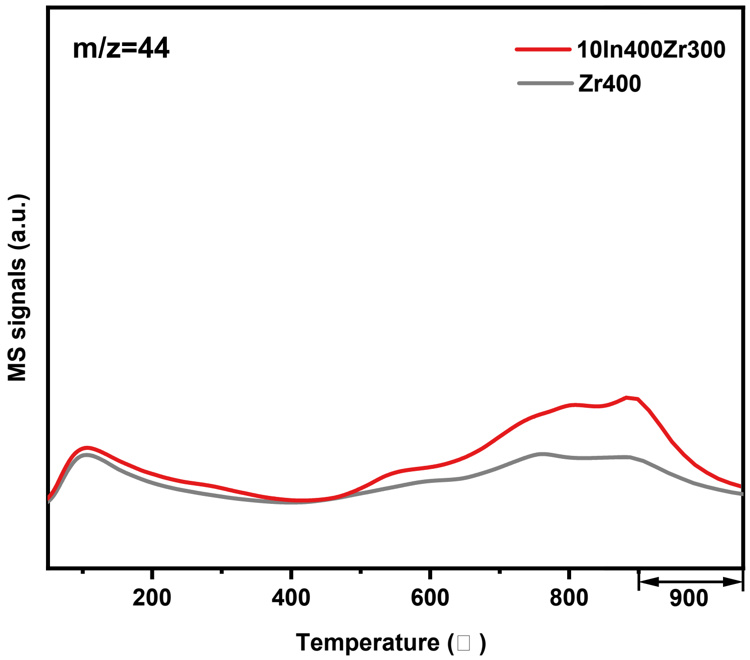

Figure S19. CO_2-TPD profiles of Zr400 and 10In400Zr300.

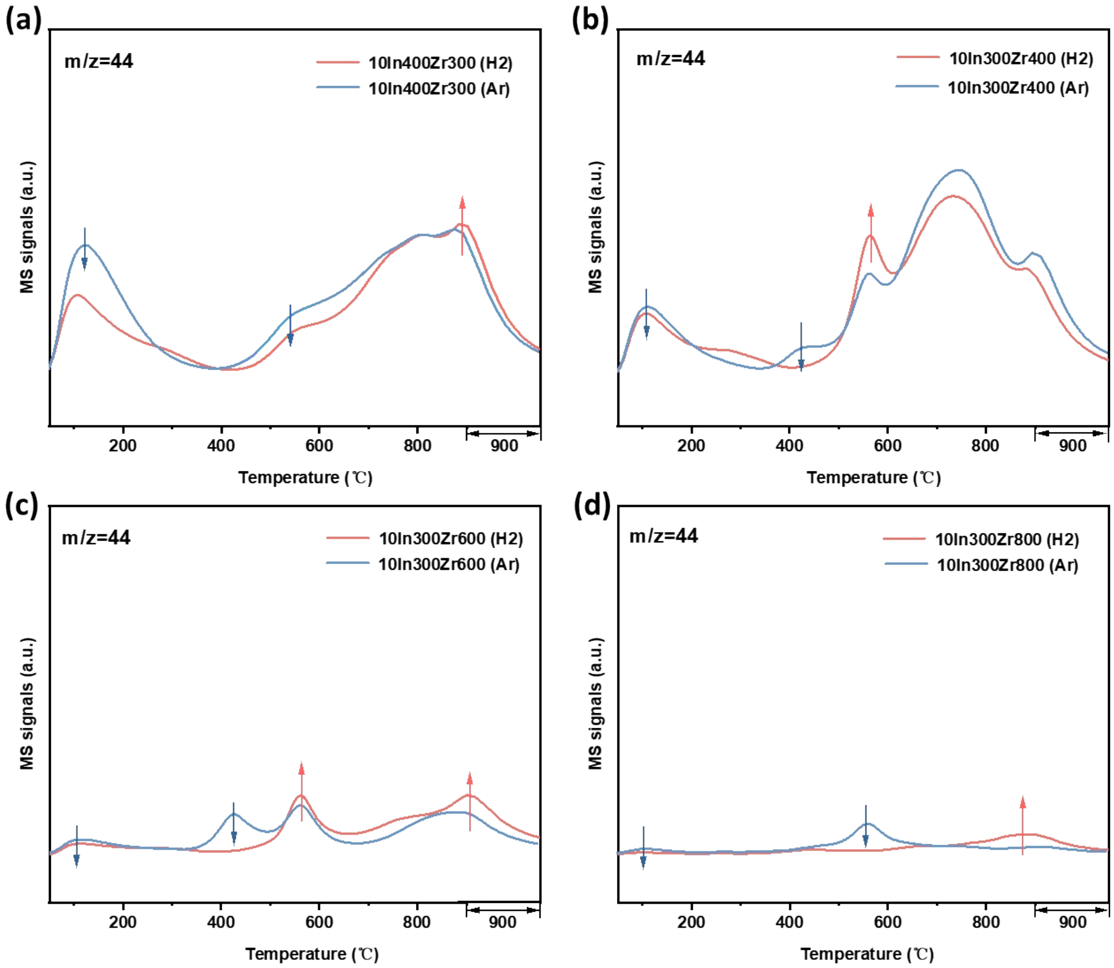

Figure S20. CO_2-TPD profiles of In_2O_3-ZrO_2 catalysts under H_2 and Ar treatments: (a) 10In400Zr300, (b) 10In300Zr400, (c)10In300Zr600, (d) 10In300Zr800.

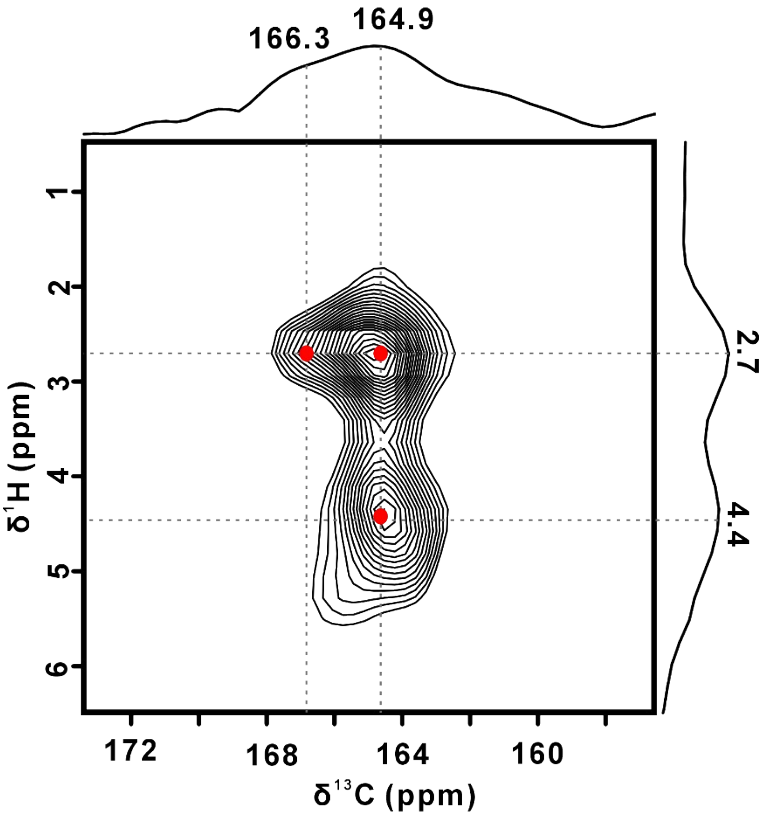

Figure S21. 2D ^{13}C-^{1}H HETCOR MAS SSNMR spectra of 10In300Zr400.

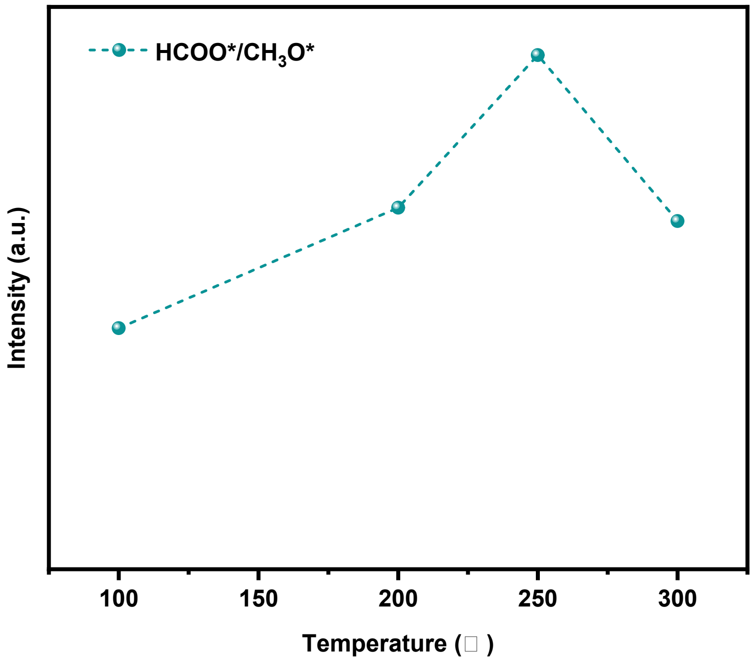

Figure S22. Profiles of IR peak intensities of $HCOO^*/CH_3O^*$ as a function of temperature.

Table S1. Physicochemical parameters of ZrO_2 supports and In_2O_3-ZrO_2 catalysts.

Catalysts	$I_{m\text{-}Zr}/(I_{m\text{-}Zr}+I_{t\text{-}Zr})$ (%) [a]	Average crystal size (nm) [b]	Indium content (wt%) [c]
Zr300	0 (a-ZrO_2)	—	—
Zr400	0 (t-ZrO_2)	9.1	—
Zr600	30	15.3	—
Zr800	90	34.6	—
10In400Zr300	0 (t-ZrO_2)	10	9.9
10In300Zr400	13	10.2	9.5
10In300Zr600	48	17.8	10.2
10In300Zr800	90	29.3	9.8

[a] the relative content of m-ZrO_2 in the ZrO_2 supports and In_2O_3-ZrO_2 catalysts, denoted as $I_{m\text{-}Zr}/(I_{m\text{-}Zr}+I_{t\text{-}Zr})$, was determined by analyzing the intensity ratios of the characteristic diffraction peaks corresponding to t-ZrO_2 (101) ($I_{t\text{-}Zr}$, ca. 30.2°) and m-ZrO_2 (-111) ($I_{m\text{-}Zr}$, ca. 28.2°).[2]

[b] the average crystal sizes were calculated using the Scherrer equation based on the diffraction peaks corresponding to the (101) plane of t-ZrO_2 and the (-111) plane of m-ZrO_2.

[c] the indium content was determined based on the results obtained from ICP-OES.

Table S2. Catalytic performance of ZrO_2, In_2O_3 and In_2O_3-ZrO_2 catalysts.

Catalysts	Temperature (°C)	CO_2 Conversion (%)	Methanol Selectivity (%)
In_2O_3	310	4.8	54.9
ZrO_2	310	0.5	0
10In400Zr300	250	1.0	95.7
	270	1.9	87.5
	290	3.7	75.6
	310	6.4	58.9
10In300Zr400	250	3.2	96.0
	270	5.4	90.0
	290	7.9	83.0
	310	10.4	73.1
10In300Zr600	250	1.7	96.9
	270	2.8	92.6
	290	4.4	83.8
	310	6.9	71.7
10In300Zr800	250	0.2	100
	270	0.4	96.3
	290	0.8	92.4
	310	1.6	87.4

Reaction conditions: 0.1 g catalyst, GHSV=12000 mL $g_{cat}^{-1} \cdot h^{-1}$, 5 MPa, H_2/CO_2=3.

Table S3. The H_2 consumption peak area in In_2O_3-ZrO_2 catalysts.

Catalysts	A_{H2} [a]	Relative consumption of H_2 (%)	Yield $_{MeOH}$ (%) [b]
10In400Zr300	0.27	32	3.68
10In300Zr400	0.82	100	7.61
10In300Zr600	0.52	63	4.95
10In300Zr800	0.17	21	1.36

[a] Peak area of H_2 consumption in H_2-TPR.

[b] Reaction conditions: 0.1 g catalyst, GHSV=12000 mL $g_{cat}^{-1}\cdot h^{-1}$, 5 MPa, 310 °C, $H_2/CO_2=3$.

Table S4. The hydroxyl groups contents on ZrO_2 supports and In_2O_3-ZrO_2 catalysts.

Catalysts	Surface acid concentration (μmol g^{-1}) [a]	μ_1-OH (μmol g^{-1})	μ_2-OH (μmol g^{-1})	μ_3-OH (μmol g^{-1})
10In400Zr300	54	5	15	34
10In300Zr400	182	19	25	138
10In300Zr600	79	10	22	47
10In300Zr800	23	7	7	9

[a] Total surface acid concentration obtained from the integral area of NH_3-TPD.[3]

References

1. T. Liu, D. Xu, M. Song, X. Hong and G. Liu, *ACS Catalysis*, 2023, **13**, 4667-4674.
2. C. Yang, C. Pei, R. Luo, S. Liu, Y. Wang, Z. Wang, Z.-J. Zhao and J. Gong, *Journal of the American Chemical Society*, 2020, **142**, 19523-19531.
3. C. Jia, X. Kan, X. Zhang, G. Lin, W. Liu, Z. Wang, S. Zhu, D. Ju and J. Liu, *Chemical Engineering Journal*, 2022, **427**, 131554.